Light scattering properties of natural and artificially demineralized dental enamel at 1310 nm

Cynthia L. Darling
Gigi D. Huynh
Daniel Fried
University of California
San Francisco, California 94143-0758
E-mail: daniel.fried@ucsf.edu

Abstract. A fundamental understanding of how near-IR light propagates through sound and carious dental hard tissues is essential for the development of clinically useful optical diagnostic systems, since image contrast is based on changes in the optical properties of these tissues on demineralization. During the caries (decay) process, micropores are formed in the lesion due to partial dissolution of the individual mineral crystals. Such small pores behave as scattering centers, strongly scattering visible and near-IR light. The optical properties of enamel can be quantitatively described by the absorption and scattering coefficients, and the scattering phase function. Our aim is to measure the optical scattering behavior of natural and artificial enamel caries. Near-IR attenuation measurements and angular-resolved goniometer measurements coupled with Monte Carlo simulations are used to determine changes in the scattering coefficient and the scattering anisotropy on demineralization at 1310 nm. An ultrahigh resolution digital microradiography system is used to quantify the lesion severity by measurement of the relative mineral loss for comparison with optical scattering measurements. The scattering coefficient increases exponentially with increasing mineral loss. Natural and artificial demineralization increases the scattering coefficient more than two orders of magnitude at 1310 nm, and the scattering is highly forward directed. © *2006 Society of Photo-Optical Instrumentation Engineers.* [DOI: 10.1117/1.2204603]

Keywords: near-infrared; light scattering; dental enamel; dental caries; scattering anisotropy.

Paper 05243R received Aug. 19, 2005; revised manuscript received Jan. 18, 2006; accepted for publication Jan. 18, 2006; published online May 25, 2006.

1 Introduction

New, more sophisticated diagnostic tools are needed for the detection and characterization of caries lesions in the early stages of development. If carious lesions are detected early enough, they can be arrested/reversed by nonsurgical means through fluoride therapy, antibacterial therapy, dietary changes, or by low intensity laser irradiation.

Dentists also need an imaging technology that can reliably track the course of caries lesions over an extended time period to determine whether the lesion is active and expanding or whether the lesion has been arrested, to determine if intervention is needed. In our laboratory, we are developing near-IR imaging methods for caries detection that exploit changes in the light scattering properties of dental enamel that occur on demineralization.[1,2]

Dental enamel manifests high transparency in the near-IR, therefore the near-IR is ideally suited for: transillumination of teeth for the detection of interproximal caries,[2] near-IR imaging of occlusal caries,[3] and for imaging with optical tomographic methods such as optical coherence tomography.[4] To ef-

fectively develop such technologies and optimize their effectiveness, it is necessary to understand how near-IR light propagates through the tooth and how the optical properties of the tooth change as a result of natural demineralization or tooth decay. The aim of this work was to determine how the scattering properties of dental enamel change with natural and artificial demineralization.

The principal factor limiting caries detection via optical imaging methods in the visible range of 400 to 700 nm is light scattering. Light scattering in sound enamel and dentin is sufficiently strong in the visible range to obscure light transmission through the tooth. The magnitude of light scattering in dental enamel is expected to decrease $(1/\lambda^3)$ due to the size of the principal scatterers in enamel. Therefore, the near-IR region from 780 to 1550 nm offers the greatest potential for new optical imaging modalities due to the weak scattering and absorption in dental hard tissue.[5] Ballistic transmission measurements have demonstrated that enamel has the highest transparency in the near-IR region near 1310 nm.[6] At this wavelength, the attenuation coefficient is only 2 to 3 cm^{-1}, a factor of 20 to 30 times lower than in the visible region. At longer wavelengths, water absorption in-

Address all correspondence to Daniel Fried, PRDS, Univ. of California—San Franscisco, 707 Parnassus Ave. San Francisco, CA 94143; Tel: 415–502–6641; Fax: 415–476–0858; E-mail: daniel.fried@ucsf.edu
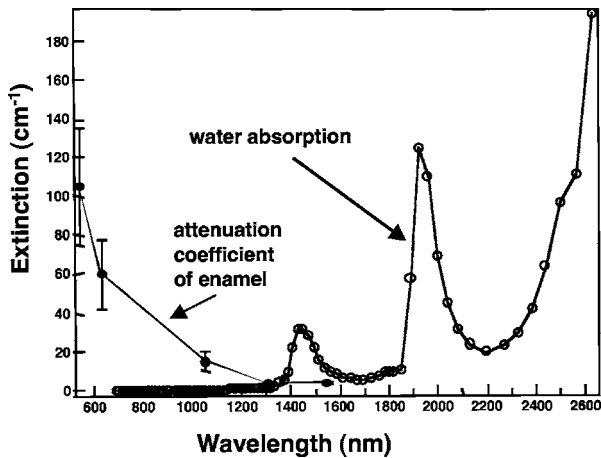
Fig. 1 Plot of the extinction (attenuation) coefficient of dental enamel (filled circles) and the absorption coefficient of water (open circles) versus wavelength.[5,6,30]

creases markedly, reducing the penetration of IR light (see Fig. 1).

Dental hard tissue optics is inherently complex due to the nonhomogeneous and anisotropic nature of these biological materials. Dental enamel is an ordered array of inorganic apatite-like crystals surrounded by a protein/lipid/water matrix. The crystals are approximately 30 to 40 nm in diameter and can be as long as 10 μm. The crystals are clustered together in 4-μm-diameter rods (or prisms), which are roughly perpendicular to the tooth surface. Because of the complex nature of these materials, the scattering distributions are generally anisotropic and depend on tissue orientation relative to the irradiating light source,[5,7–9] in addition to the polarization of the incident light.

The optical parameters for normal enamel and dentin have been reported between the wavelength range of 200 to 700 nm. For enamel, absorption is very weak in the visible range ($\mu_a < 1$ cm^{-l}, $\lambda = 400$ to 700 nm) and increases in the ultraviolet ($\mu_a > 10$ cm^{-1}, $\lambda < 240$ nm).[10] For dentin in the 400 to 700 nm wavelength range, the absorption coefficient is essentially wavelength independent with a value of $\mu_a \sim 4$ cm^{-1}.[11] The optical properties of normal enamel and dentin, including the scattering phase function and anisotropy, were determined at 1053, 632, and 543 nm using angular resolved light scattering measurements and Monte Carlo (MC) simulations of light propagation.[5]

The optical properties of biological tissue can be quantitatively described by defining the optical constants, the absorption (μ_a) and scattering coefficients (μ_s), which represent the probability of the incident photons being absorbed or scattered, and the scattering phase function $\Phi[\cos(\theta)]$, which is a mathematical function that describes the directional nature of scattering.[12–14] With knowledge of these parameters, light transport in dental hard tissue can be completely characterized and modeled. Accurate description of light transport in dental hard tissue relies on knowledge of the exact form of the phase function $\Phi[\cos(\theta)]$ for each tissue scatterer at each wavelength.[14] Therefore, direct measurement of the phase function is necessary. It is important to note that the empirically derived Kubelka-Munk (KM) coefficients that are com-

monly used in dentistry are not normal fundamental optical constants and are not appropriate for describing light transport in tissues with highly forward directed scattering such as enamel and dentin, particularly in the near-IR.[12–15] Van der Zee[15] compared KM methods with Monte Carlo methods and found that the KM method led to considerable errors and that it was necessary to use the more rigorous MC method for accurate results.

We demonstrated previously that angular resolved scattering distributions of enamel and dentin representing single scattering could be measured. This was experimentally achieved by using thin sections with a thickness much less than the photon mean free path (MFP), to ensure single scattering, and an index-matching bath to remove the influence of surface scattering and refractive effects. The optical properties were subsequently determined using Monte Carlo simulations of photon transport. Although this approach is laborious and computationally intensive, it has been shown consistently to yield the most reliable values.[12,14] The accuracy of the values computed was confirmed by successfully modeling the angular resolved scattering distributions measured for sections of various thickness from 100 μm to 2 mm in the multiple scattering regime. Applying this method, we were able to accurately determine the optical constants and the scattering phase function for sound enamel and dentin at 543, 632, and 1053 nm.[5,16] More recently, we measured the attenuation coefficient μ_t, which is the sum of the scattering and absorption coefficients at 1310 and 1550 nm.[6] Measurement of the enamel attenuation coefficient at 1310 and 1550 nm posed a particular challenge, since the scattering coefficient is almost two orders of magnitude lower than in the visible range, ~ 3 cm^{-1} at 1310 nm versus 105 cm^{-1} at 543 nm. Moreover, surface scattering can completely mask the measurement of the bulk scattering properties.[5]

The measured angular resolved scattering distributions could not be represented by a single scattering phase function $\Phi(\cos \theta)$, and required a linear combination of a highly forward peaked phase function, a Henyey-Greenstein (HG) function, and an isotropic phase function represented by the following equation:[5]

$$\Phi(\cos \theta) = f_d + (1 - f_d)\left[\frac{(1 - g^2)}{(1 + g^2 - 2g \cos \theta)^{3/2}}\right]. \quad (1)$$

The parameter f_d for fraction diffuse is defined as the fraction of isotropic scatter. The average value of the cosine of the scattering angle (θ) is called the scattering anisotropy (g), and $g = 0.96$ and $g = 0.93$ for enamel and dentin, respectively, at 1053-nm.[5]

The fraction of isotropic scatter (f_d) was measured to be 36% for enamel and less than 2% for dentin at 1053 nm. Due to the heterogeneous structure of dental hard tissues, the phase function changes with wavelength; therefore, the phase function has to be independently determined at each wavelength. Angular resolved scattering measurements on a 2-mm-thick section of sound enamel at 1310 nm previously coupled with Monte Carlo simulations yielded a HG function with $g = 0.96$ and $f = 55\%$ isotropic scattering.[17] The scattering coefficient used in those simulations was 3 cm^{-1}. It is interesting to note that the shape of the scattering distributions measured

at 1310 nm is similar to those measured at 1053 nm. with the exception of the markedly higher dynamic range ~ 100 db, and minimal reduction in the ballistic light transmitted at 0 deg. For comparison, at 543 nm the ballistic component at 0 deg was no longer visible in sections greater than 1 mm thickness, and the diffuse (multiply scattered component) at angles greater than 5 to10 deg was of similar magnitude. At 1310 nm, the ratio of intensity of the unscattered component is still 50 dB or five orders of magnitude higher than the diffuse component for the sample of 2 mm thickness.

The nature of the scattering phase function suggests that there are two types of scatterers in enamel and dentin. We hypothesize that the small enamel crystallites of less than 50 nm in diameter produce Rayleigh-like isotropic distributions and are responsible for the large fraction of isotropic scattering from the tissue. The large enamel prisms and dentinal tubules that are a few microns across are Mie-like scatterers, producing highly forward directed scattering distributions that can be described by a HG function, the second term in Eq. (1). We also postulate that demineralization will substantially increase the fraction of isotropic scatterers (f_d) and increase the amount of large angle scattering from the carious lesion. To test this hypothesis, the angular distribution of scattered light was measured in thin sections of enamel exposed to a pH cycling regimen to produce artificial or simulated caries lesions.

The first step to determining the optical properties of carious enamel is to establish a method of characterizing the severity of the carious lesion. The gold standard in cariology research is mineral loss, which defines the degree of demineralization in the lesion. The most severe lesions have lost a higher volume fraction or volume percent of their original mineral content than less severe lesions. We have assembled, tested, and calibrated a high-resolution digital microradiography (DM) system—spatial resolution 2.1 μm—for quantification of lesion severity (Fig. 2). The DM system allows real-time acquisition of digital x-rays and works well for thicker sections, greater than the 80-μm thin sections typically required for conventional film-based microradiography. This is a major advantage, since it is difficult to cut 80-μm thin sections without destroying natural lesions, and grinding and polishing modifies the soft lesion.

Increased backscattering from the demineralized region of early caries lesions is the basis for the visual appearance of white spot lesions.[18,19] An increase in porosity of the lesion leads to increased scattering at the lesion surface and higher scattering in the body of the lesion, producing an increase in the magnitude of the diffuse reflectance.[20] Attempts at measuring the optical properties of dental caries have been limited to measurements of backscattered light from optically thick, multilayered sections of simulated caries lesions.[20–22] The microstructure of enamel and dentin caries lesions is complex, consisting of various turbid and transparent zones.[23,24] Demineralized areas of coronal caries appear whiter and are more opaque. During remineralization, pores and tubules are filled with minerals, and those areas are typically more transparent. There have been some attempts to measure and simulate light scattering in artificial and natural lesions.[18,22,25] However, to our knowledge there has not been a major effort to measure and quantify the optical properties of carious lesions in terms
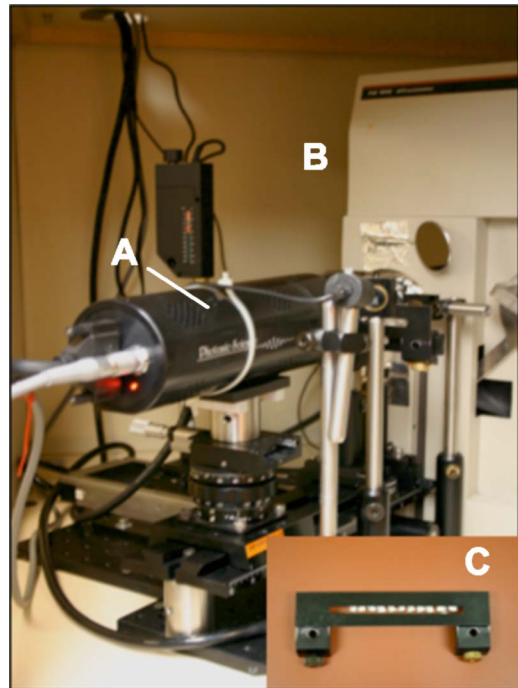

Fig. 2 High-resolution digital x-ray microradiography system (DM), (a) FDI x-ray imager with motion control system, (b) x-ray diffractometer, and (c) sample mount.

of changes in the fundamental optical constants μ_s and μ_a and the scattering phase function. In this study, we have used lasers, precision positioning stages, and a zoom video microscope system to accurately position the laser beam with a spot size of 50 to 100 μm on various areas of carious lesions for direct comparison with matching acquired DM images. One procedural difference between measuring carious lesion areas versus sound tissue areas is the method of index matching. Lesion areas are highly porous, allowing index matching fluids to imbibe into the lesion, effectively eliminating the lesion from an optical standpoint, i.e., the lesion becomes more transparent than the sound tissue. Our method is predicated on the principle that carious lesions will be filled with fluid in their natural state, and that measurement in water replicates the conditions that will be encountered clinically.

2 Materials and Methods

2.1 Natural Lesions

Teeth extracted from patients in the San Francisco Bay area were collected, cleaned, and sterilized with gamma radiation. The teeth were inspected, and 200-μm-thick sections were cut through suspected interproximal and occlusal caries lesions identified by visual inspection. The thickness of each section was measured with a digital micrometer with 1-μm resolution. Ideally, thin sections of 80- to 100-μm thickness should be used for both polarized light microscopy and DM; however, enamel is very brittle and difficult to cut into thin sections without fracture, more so for carious sections, and attempts to produce such thin sections would result in an unacceptable high loss rate of samples/sections. Therefore, we chose a more reliable section thickness of 200 μm.
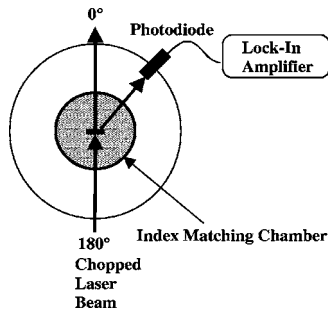
Fig. 3 Automated goniometer with index matching bath to measure angular resolved scattering distributions

Fig. 5 Near-IR imaging setup: (a) InGaAs FPA, (b) cuvette and section holder, (c) aperture, (d) neutral density filters, and (e) laser fiber pigtail and collimator.

2.2 Simulated-Caries Lesions

Simulated caries lesions were produced in 200-μm-thick human tooth sections using well-characterized demineralizing and remineralizing solutions for varying time periods to produce simulated caries lesions of varying severity. The pH cycling model that replicates the cycle of demineralization and remineralization that takes place naturally in the mouth as the pH fluctuates before and after meals[26,27] was used. Both sides of human tooth sections were exposed for 1, 2, 3, 4, and 5 days to a daily regimen of 6-h demineralization by 17-h remineralization (see Fig. 3). A total of five sections were used and the scattering distributions were measured after each full daily period of pH cycling. In the pH cycling model, a surface zone is created due to the protection of the surface layer, and erosion does not occur as the lesion progresses in depth. Each section was immersed in 40-mL aliquots of a buffer solution containing 2.0-mmol/L calcium, 2.0-mmol/L phosphate, and 0.075-mol/L acetate maintained at pH 4.3 and a temperature of 37°C for a period of 6 h each day, followed by immersion in a remineralization solution overnight for 17 h in a solution of 1.5-mmol/L calcium, 0.9-mmol/L phosphate, 150-mmol/L KCl, and 20-mmol/L cacodylate buffer maintained at pH 7.0 and 37°C. Figure 4 shows diagrammatically how the demineralized zone advances in the section overtime. After 6 days, some of the samples cavitated as the simulated lesion advanced completely through the section.

2.3 Digital Microradiography

A custom-built digital microradiography (DM) system was used to measure mineral loss in the natural caries lesions. High-resolution microradiographs were taken using Cu K$_a$ radiation from a Philips 3100 x-ray generator and a Photonics
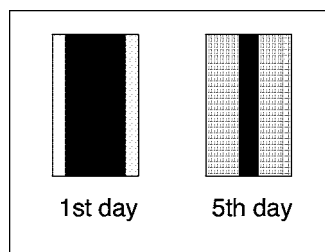
Fig. 4 Schematic of the tooth sections of 200-μm section after 1 and 5 days of pH cycling. The dark zone is sound enamel while the outer zone is the demineralized area.
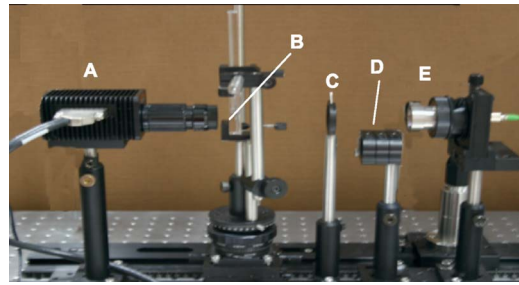
Science FDI x-ray digital imager (Microphotonics, Allentown, Pennsylvania). The x-ray digital imager consists of a 1392 $\times$ 1040-pixel interline charge-coupled device (CCD) directly bonded to a coherent micro-fiber optic coupler that transfers the light from an optimized gadolinium oxysulphide scintillator to the CCD sensor. The pixel resolution is 2.1 μm and images can be acquired in real time at a frame rate of 10 fps. The image size is 2.99$\times$2.24 mm with a pixel resolution of 2.15 μm. A high-speed motion control system with Newport UTM150 and 850G stages and an ESP300 controller coupled to a video microscopy and laser targeting system was used for precise positioning of the tooth samples in the field of view of the imaging system. The setup is shown in Fig. 2. The volume percent mineral content of each section was determined by comparison with a calibration curve of x-ray intensity versus sample thickness created using sound enamel sections of 86.3$\pm$1.9% volume percent mineral varying from 50 to 300-μm in thickness. This approach was validated via comparison with cross sectional microhardness measurements. The volume percent mineral determined using microradiography for section thickness ranging from 50 to 300 μm highly correlated with the volume percent mineral determined using microhardness $R^2=0.99$.

2.4 Near-Infrared Attenuation Measurements and Images

The optical imaging system used in this study is a InGaAs focal plane array (318$\times$252 pixels), the Alpha NIR™ (Indigo Systems, Goleta, California) with an infinimite™ lens (Infinity, Boulder, Colombio). Light from a single-mode fiber pigtail coupled to a 1310-nm superluminescent diode (SLD) with an output power of 15 mW and a 35-nm bandwidth, model SLED1300D20A (Optospeed, Zurich, Switzerland), was coupled to a 20-mm NIR fiber collimator (μLS Micro Laser Systems, Garden Grove, California). Neutral density filters were used to attenuate the incident laser beam. The sample was mounted on an acrylic post and inserted in a cuvette filled with deionized water. The acquired 12-bit digital images were analyzed using IR Vista™software (Indigo Systems, Goleta, California). The setup is shown in Fig. 5.

2.5 Goniometer Measurements

An automated goniometer with 0.01-deg resolution was constructed to rotate an amplified germanium photodiode detector, PDA400 (Thorlabs, Newton, New Jersey) around fixed
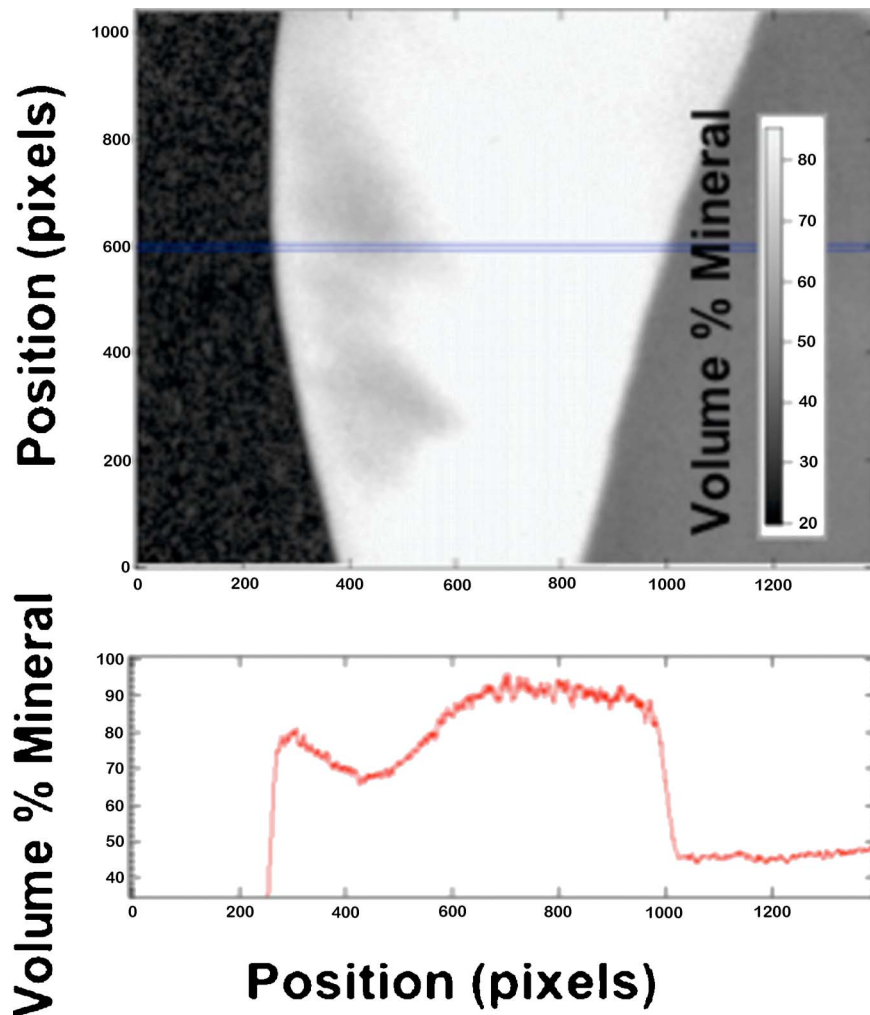
Fig. 6 (top) A high-resolution digital microradiograph of the lesion area shows the volume percent mineral versus position in the lesion. (bottom) Volume percent mineral versus position for the horizontal line drawn through the lesion.

tissue sections immersed in an index matching bath (see Fig. 3). A 1310.00-nm distributed feedback (DFB) laser with a 20-mW output (NTT Electronics Corporation, Tokyo, Japan) was focused onto the section with a spot size of 100 μm. The laser current was modulated at 2 kHz using a LDC 2000 diode controller and TEC 2000 temperature controller both from Thorlabs, (Newton, New Jersey) and synchronized to an SR850 digital lock-in amplifier (Stanford Research Systems, Stanford, California). The digital lock-in amplifier enables a dynamic range of 100 dB for high sensitivity. A quartz cylindrical index-matching saline bath was used to remove the influence of surface scattering and total internal reflection on the bulk scattering properties. A 670-nm pigtailed diode was combined with the 1310-nm laser pigtail using a 1×2 optical fiber coupler before the output was focused onto the tooth sections. The coaxial laser beams, one visible, allowed exact positioning of the near-IR laser beam on each section. A video microscope was used to monitor position on a video display.

The angular resolved scattering distributions were subsequently fitted using Monte Carlo methods to estimate the scattering coefficient and phase function.[28] The program of Wang and Jacques was used, employing the phase function shown in

Eq. (1) to calculate the simulated angular resolved scattering distributions for comparison with those measured using the scattering goniometer.[29]

3 Results

Digital microradiography and near-IR transillumination images of each tooth section with a clearly identified lesion area were acquired. Angularly resolved goniometer measurements were subsequently taken at selected locations in both lesion and sound areas of the tooth section. We present measurements on ten such tooth sections taken from ten natural lesions. The tooth sections were approximately 200 μm thick. The microradiographs for the first lesions are shown in Fig. 6. Figure 6 contains an image of the processed x-ray data that is presented as volume percent mineral—sound enamel is approximately 91% vol.% mineral. The line profiles shown in the bottom of Fig. 6 were taken across the lesion and reflect the severity and topography of the lesion. Goniometer measurements from the tooth section shown in Fig. 6 yielded μ_s =9, g=0.98, and f=0.25 for the sound enamel (91% mineral), and μ_s=190, g=0.97, and f=0.10 for the most dem-
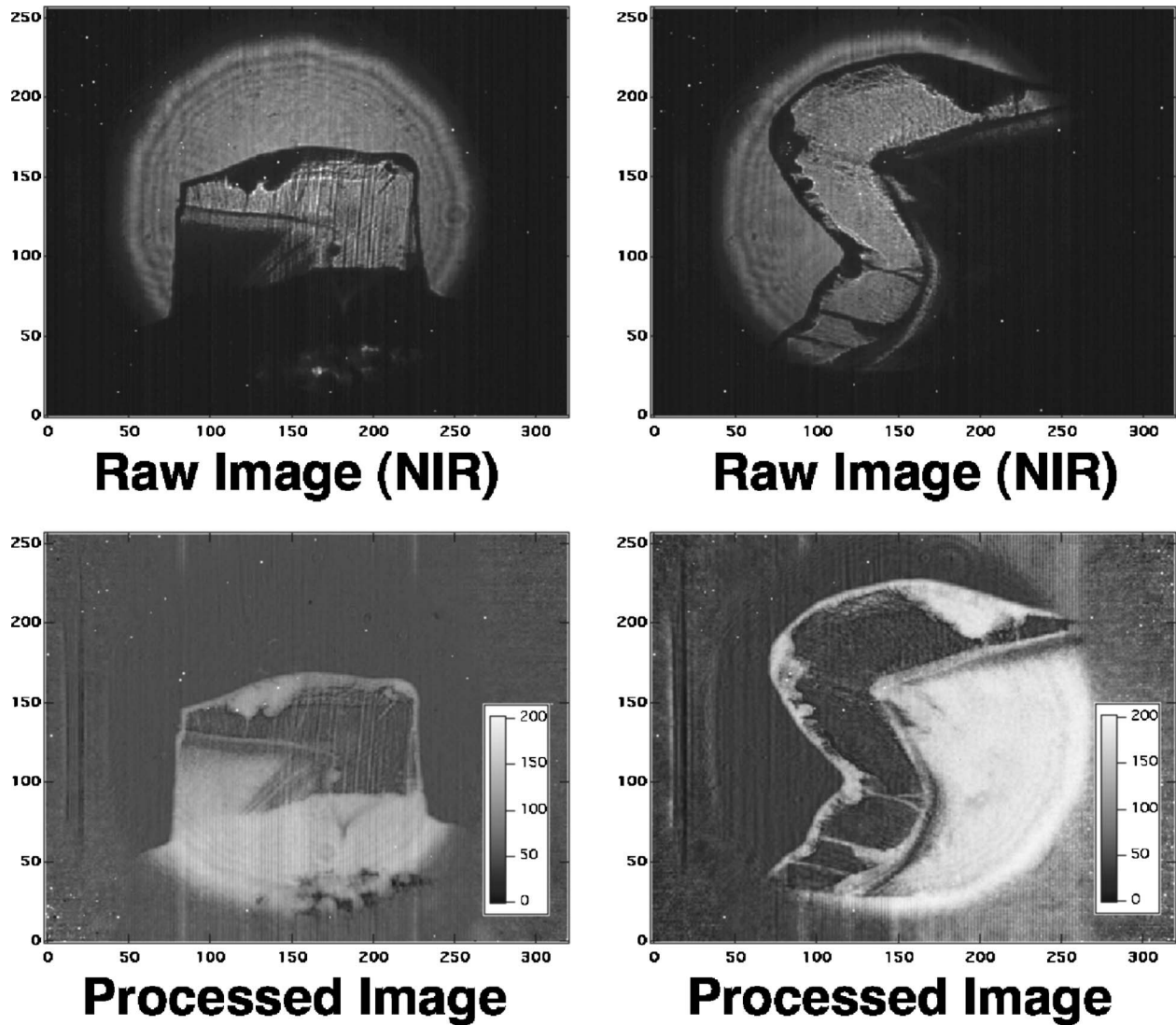
Fig. 7 (top) Unprocessed images of near-IR (1310 nm) and (bottom) processed images of NIR optical attenuation through a 160-μm (left) and 230-μm (right) thick tooth sections with natural caries lesions are displayed. The attenuation coefficient is in units of cm^{-1} and ranges from 0 to 200.

ineralized region (68% mineral). Entire near-IR images of the optical attenuation through the tooth sections were acquired using a large fiber collimator (20-mm beam diameter) and an InGaAs focal plane array (FPA). Those images are shown in Fig. 7. Two images are displayed, the top images are the raw intensity images and the lower images represent the attenuation through the sample, which is calculated using the background intensity image, the section thickness, and Beer's law. The white areas in the processed images represent more opaque regions, and the dark areas are more transparent. The attenuation in the lesion approaches 100 to 200 cm^{-1}, a factor of 1 to 2 orders of magnitude higher than the surrounding sound enamel, i.e., 2 to 3 cm^{-1}, and is a similar magnitude to that of the more highly scattering dentin. The absorption coefficient of water at 1310 nm is 1.2 cm^{-1},[30] and enamel is 8 to 10% water, therefore the absorption coefficient is assumed to be approximately 0.12 cm^{-1}, a factor of 20 to 30 less than

the scattering coefficient, hence we assume that it is negligible.

Angularly resolved scattering measurements were taken from three points of varying mineral content in the lesion of Fig. 8. One point was the sound enamel (85% mineral), the second point was taken in the less severely demineralized surface zone (78% mineral), and the third point was taken from the most severely demineralized part of the lesion, marked A in Fig. 9, that is 68% mineral. The ballistic light is reduced by two orders of magnitude and the intensity of the light scattered at angles greater than 10 deg is 3 to 4 orders of magnitude higher for the carious tissue over the sound enamel. The angular-resolved goniometer measurements and the corresponding Monte Carlo simulations are shown in Fig. 9. The parameters $\mu_s=3.0$, $g=0.96$, and $f=0.3$ fit the sound enamel (85% mineral) quite well. In the surface zone marked B (78% mineral) in Fig. 9, the parameters $\mu_s=30$, $g=0.90$,
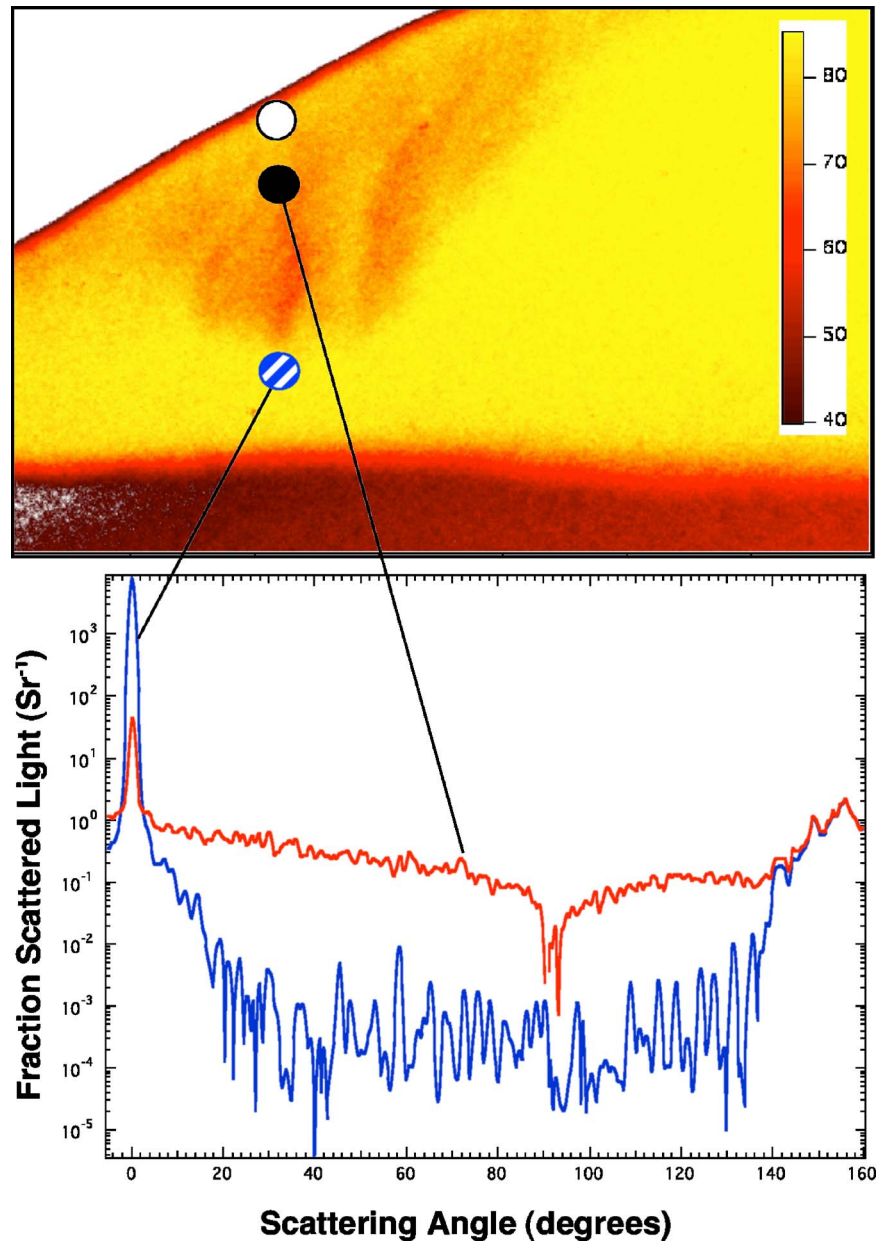
Fig. 8 (top) A high-resolution digital microradiograph of the lesion area shows the volume percent mineral versus position in the lesion area. (bottom) The fraction of NIR (1310 nm) light scattered versus angle in the sound (blue) and carious (black) areas of the sample measured with the scattering goniometer. Monte Carlo simulations of those goniometer measurements are shown in Fig. 9 (open circle in surface zone is caries in Fig. 9(A), filled circle in lesion body is caries in Fig. 9(B) and cross hatched circle is sound enamel in both Figs 9(A) and 9(B)).

and $f=0.55$ were used to provide the best fit, while in the most severely demineralized zone in Fig. 9(A) (68% mineral), the parameters $\mu_s=250$, $g=0.95$, and $f=0.55$ provided the best fit.

Similar NIR and DM images were acquired from ten caries lesions, and a plot of the optical attenuation versus volume percent mineral loss for ten data points assembled from all the line-profiles across the most highly demineralized area of each lesion are shown in Fig. 10 (note points from each independent sample follow a similar behavior). Nonlinear regression using an exponential growth curve shows that the optical scattering increases exponentially with mineral loss and that the magnitude of light scattering approaches a maximum after

10 to 15% mineral loss, which is consistent with the formation of pores. For higher volume percent mineral loss, additional pores interconnect and the enamel falls apart, forming a cavity above 40 to 50% mineral loss.

3.1 Artificial Lesions

Angular resolved scattering measurements measured during the development of enamel lesions over a period of five days of pH cycling also show exponential growth. There is a rapid order of magnitude increase in optical scattering after just 1 day of lesion growth, followed by a slower increase of another order of magnitude after the next 4 days.
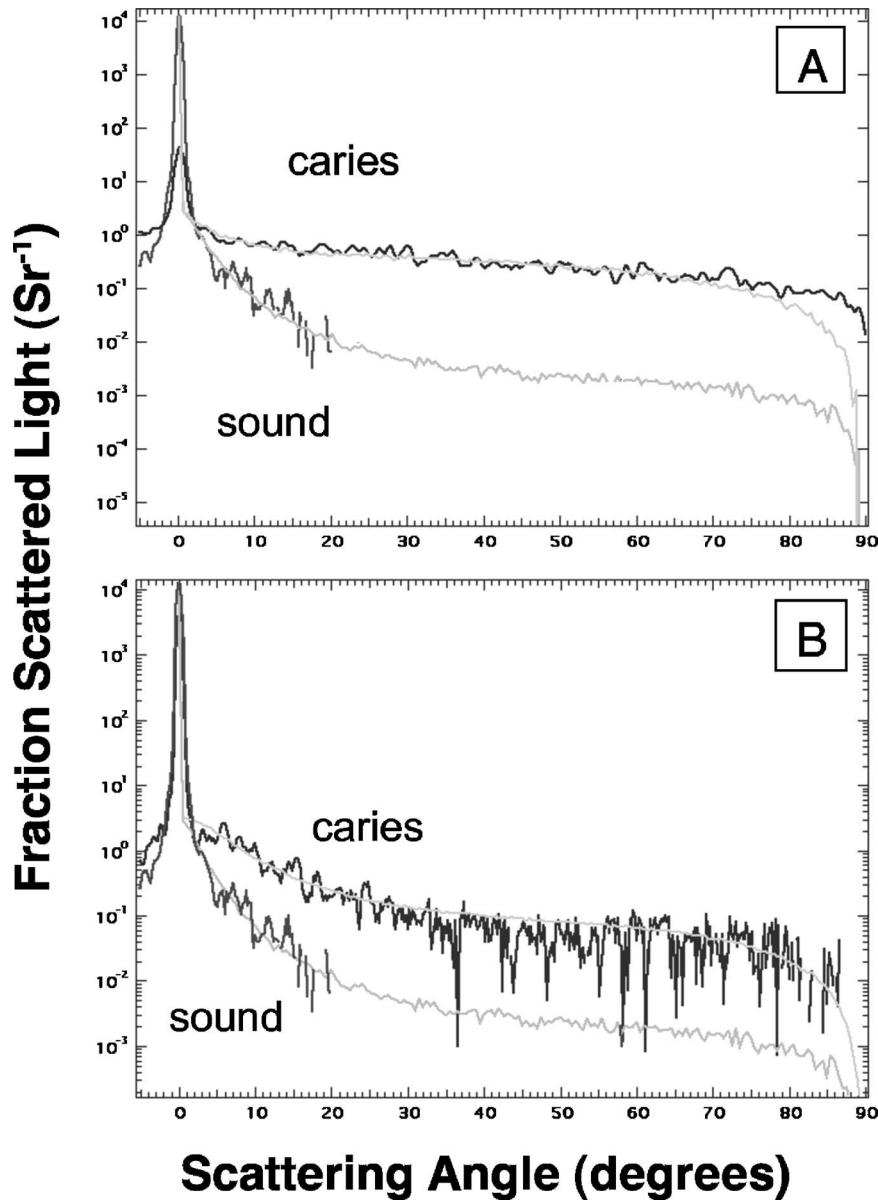
Fig. 9 Angular-resolved scattering measurements of sound enamel and carious enamel taken at three positions of varying demineralization in the caries lesion of Fig. 8. Graph A shows the scattering lesion body (filled circle in Fig. 8). Graph B shows scattering from the lesion surface zone (open circle in Fig. 8). The best fit MC simulations are shown as well and the parameters are listed in the text for the MC simulations.

One of the angularly resolved scattering distributions measured at 1310 nm after exposure to five days of a pH cycling regimen is shown in Fig. 11, along with the same section before lesion formation (sound enamel). The ballistic transmission falls by 2 to 3 orders of magnitude after lesion formation. Although the scattered light appears at larger angles, the scattering distribution is far from isotropic in contrast to our predictions. Apparently, the scattering caused by the pores formed in the enamel as a result of demineralization is highly forward directed. Figure 12 shows the average scattering distributions measured for all five sections after 0 to 5 days of pH cycling. The most dramatic change in the scattering distributions occurred after only one day of pH cycling. Both the dip and rise past 130 deg on the scattering distributions is caused by internal reflection of the laser light and refocusing

by the scattering chamber, and is not real structure in the scattering distribution.

The Monte Carlo method was employed to determine the scattering coefficient and the parameters of the scattering phase function that best fit the average curves of Fig. 12, which represent the progressively more demineralized enamel after each day of cycling. Those data are shown in Table 1. The measured angular resolved scattering distribution used is a linear combination of a highly forward peaked phase function $\Phi(\cos \theta)$, a Henyey-Greenstein (HG) function g, and an isotropic phase function f_d represented by Eq. (1). It is important to point out that the samples were immersed in saline and therefore we were unable to eliminate contributions from surface scattering. Surface scattering would be expected to influence all of the optical parameters to some degree.
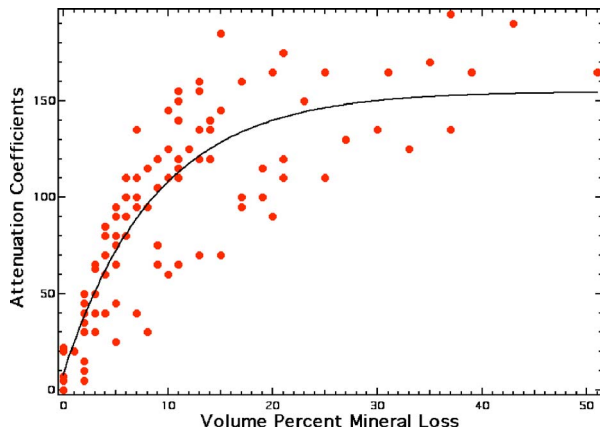
Fig. 10 Optical attenuation (cm^{-1}) at 100 points taken from ten natural enamel caries lesions (10 points per lesion). The solid line represents the best exponential fit, $r^2 = 0.74$ to the attenuation coefficient versus volume percent mineral loss.

4 Discussion

During the caries process, pores are formed in the lesion due to partial dissolution of the individual mineral crystals. Such small pores act as scattering centers, strongly scattering visible and near-IR light. These measurements indicate that such porosity caused by preferential dissolution in the lesion increases the scattering coefficient by 1 to 2 orders of magnitude higher over the sound tissue. Higher attenuation would be expected for samples that were not immersed in water due to the higher difference in refractive index of air in the porous enamel. The goniometer measurements indicate that a large fraction of the scattered light in the lesion is highly forward directed in contrast to our original hypothesis. This is not entirely unexpected, since demineralization proceeds along the core of the enamel rods, hence the scattering centers may be fairly large in the micron range and highly anisotropic. This also suggests that many of the pores in the lesion are Mie-like scatterers with scattering centers of a similar dimension to the enamel prisms. Such an observation is important for the interpretation of optical coherence tomographic images, since the lesion contrast is due to an increase in backscattered light from the lesion area.

The problem of discriminating between surface scattering and bulk scattering is important for measuring accurate values for the scattering coefficient of sound dental hard tissues. Samples are immersed in an index matching bath of exactly the same refractive index to reduce the effect of surface scattering. In addition, a Beer-Lambert plot of transmission through the tissue versus tissue thickness is used to remove the influence of surface scattering and any other extrinsic factors. Such an approach is not possible, since carious lesions are both highly variable in mineral content and are highly porous. Due to the high porosity, any index matching agent imbides into the lesion, rendering the lesion transparent. Moreover, since the lesion is optically rough and porous, the surface is an intrinsic part of the lesion that cannot be differentiated from the bulk. Therefore, we have taken the approach of measuring the optical attenuation through sections immersed in water to replicate optical conditions appropriate for the oral environment. However, it is important not to forget that the influence of surface scattering has not been decoupled from the scattering in the bulk of the lesion in these measurements. The optical attenuation through the sound regions of the tooth sections varied between 1 to 30 cm^{-1} due to the influence of surface scattering. The increase in scattering with demineralization was so profound, however, that variations in surface scattering did not prevent the elucidation of the rela-
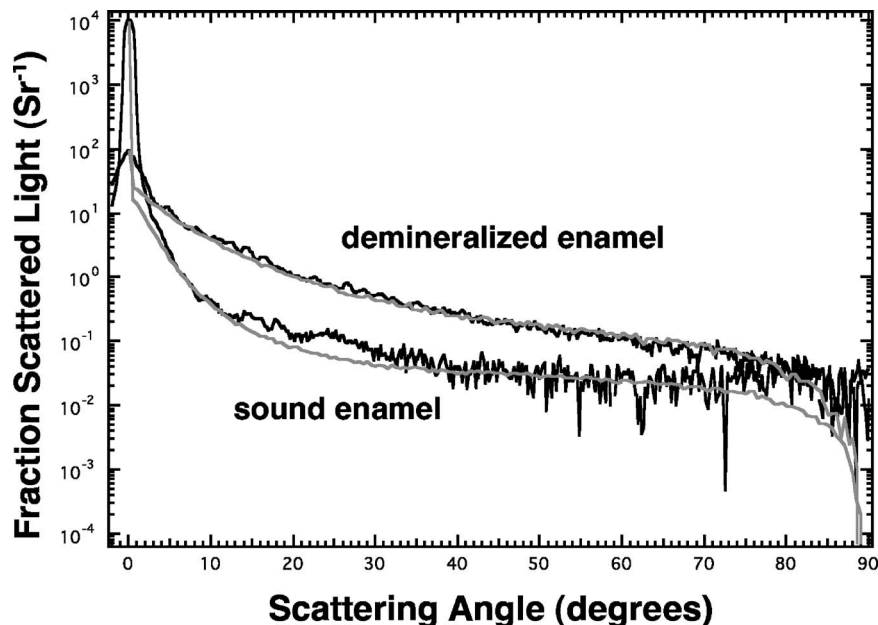
Fig. 11 Comparison of angularly resolved scattering distributions measured for sound enamel and demineralized enamel produced by exposure to five days of a pH cycling regimen. The MC simulations are shown for sound enamel (day 0) $\mu_s = 10$, $g = 0.96$, and $f = 0.45$, and carious enamel (day 5) $\mu_s = 245$, $g = 0.97$, and $f = 0.05$ provided the best fit.
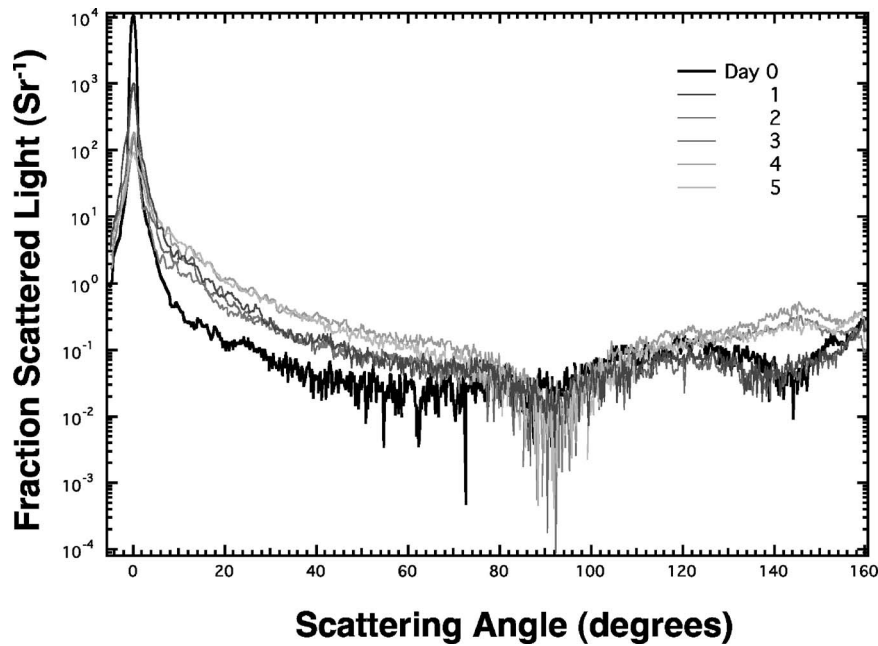
Fig. 12 Angularly resolved scattering distributions of 200-μm-thick sections of enamel exposed to pH cycling for a 0 to 5 day section measured at 1310 nm. Each trace represents the average of five measurements on five different samples.

tionship between the volume percent mineral loss and the attenuation coefficient.

The lesions manifest greater contrast between the sound and carious enamel in the near-IR attenuation measurements than in the microradiographs. The image contrast between sound and demineralized enamel in the near-IR due to changes in light scattering is much higher than the image contrast provided by variations in tissue density that occurs at x-ray wavelengths, which provides the image contrast in dental radiography. Therefore, we expect near-IR imaging methods to be more sensitive to early demineralization than x-rays. This is encouraging, since better contrast between sound and demineralized enamel should enable earlier detection of enamel demineralization. The near-IR and the polarized light microscopy images of the lesions are typically more uniform than the microradiographs, which suggests that there is a non-linear relationship between the mineral loss and the scattering coefficient, namely a large increase in scattering with slight demineralization, followed by a minimal increase in scattering for more severe lesions. The optical property measurements during the longitudinal development of early artificial demineralization suggested a similar rapid exponential increase in optical scattering during initial lesion development, followed by a more gradual increase in scattering as the lesion severity increases.[31]

In summary, we have established a method for quantifying the optical properties of sound and carious dental hard tissues, employing a combination of optical attenuation measurements, angular resolved goniometer measurements, and MC simulations that can be compared with the local mineral loss measured using high resolution digital microradiography. Using these methods, we will be able to sample lesion areas of varying mineral density in the same lesion and produce plots of mineral loss versus optical attenuation, and use such data to establish the relationship between optical scattering and lesion severity.

Table 1 Best fit Monte Carlo simulations for day 0 to 5 of each trace in Fig. 12 using the phase function in Eq. (1).

Day	μ_s	g	f
0	10	0.96	0.45
1	115	0.97	0.10
2	120	0.97	0.10
3	180	0.97	0.10
4	220	0.97	0.10
5	245	0.97	0.05

References

1. D. Fried, J. Xie, S. Shafi, J. Featherstone, T. M. Breunig, and C. Q. Le, "Imaging caries lesions and lesion progression with polarization optical coherence tomography," *Proc. SPIE* **4610**, 113–124 (2002).
2. R. S. Jones, G. D. Huynh, G. C. Jones, and D. Fried, "Near-IR transillumination at 1310-nm for the imaging of early dental caries,"*Opt. Express* **11**, 2259–2265 (2003).
3. C. M. Bühler, P. Ngaotheppitak, and D. Fried, "Imaging of occlusal dental caries (decay) with near-IR light at 1310-nm," *Proc. SPIE* **5687**, 125–131 (2005).
4. D. Fried, J. Xie, S. Shafi, J. D. B. Featherstone, T. Breunig, and C. Q.

Lee, "Early detection of dental caries and lesion progression with polarization sensitive optical coherence tomography," *J. Biomed. Opt.* **7**(4), 618–627 (2002).

5. D. Fried, J. D. B. Featherstone, R. E. Glena, and W. Seka, "The nature of light scattering in dental enamel and dentin at visible and near-IR wavelengths," *Appl. Opt.* **34**, 1278–1285 (1995).

6. R. S. Jones and D. Fried, "Attenuation of 1310-nm and 1550-nm laser light through sound dental enamel," *Proc. SPIE* **4610**, 187–190 (2002).

7. J. R. Zijp and J. J. ten Bosch, "Angular dependence of HeNe laser light scattering by bovine and human dentine," *Arch. Oral Biol.* **36**, 283–289 (1991).

8. J. R. Zijp and J. J. ten Bosch, "Theoretical model for the scattering of light by dentin and comparison with measurements, "*Appl. Opt.* **32**, 411–415 (1993).

9. J. R. Zijp, J. J. ten Bosch, and R. A. Groenhuis, "HeNe laser light scattering by human dental enamel," *J. Dent. Res.* **74**, 1891–1898 (1995).

10. D. Spitzer and J. J. ten Bosch, "The absorption and scattering of light in bovine and human dental enamel," *Calcif. Tissue Int.* **17**, 129–137 (1975).

11. J. J. ten Bosch and J. R. Zijp, *Dentine and Dentine Research in the Oral Cavity*, pp. 59–65, IRL Press, Oxford, England (1987).

12. W. Cheong, S. A. Prahl, and A. J. Welch, "A review of the optical properties of biological tissues," *IEEE J. Quantum Electron.* **26**, 2166–2185 (1990).

13. B. C. Wilson, M. S. Patterson, and S. T. Flock, "Indirect versus direct techniques for the measurement of the optical properties of tissues," *Photochem. Photobiol.* **46**, 601–608 (1987).

14. V. Tuchin, *Tissue Optics: Light Scattering Methods and Instruments for Medical Diagnostics*, SPIE Press, Bellingham, WA (2000).

15. P. van der Zee, "Methods for measuring the optical properties of tissue in the visible and near-IR wavelength range," Medical Optical Tomography:Functional Imaging and Monitoring, Vol. **IS11**, pp. 450–472, Bellingham, WA (1993).

16. D. Fried, J. D. B. Featherstone, R. E. Glena, B. Bordyn, and W. Seka, "The light scattering properties of dentin and enamel at 543, 632, and 1053 nm," *Proc. SPIE* **1880**, 240–245 (1993).

17. D. Fried, R. Jones, J. Xie, J. Featherstone, C. Darling, T. Breunig, and C. Le, "Early caries detection with PS-OCT," *Early Detection of Dental Caries III*, pp, 69–88, Indianapolis, IN (2004).

18. J. Brinkman, J. J. ten Bosch, and P. C. F. Borsboom, "Optical quan-

tification of natural caries in smooth surfaces of extracted teeth," *Caries Res.* **22**, 257–262 (1988).

19. J. J. ten Bosch, H. C. van der Mei, and P. C. F. Borsboom, "Optical monitor of in vitro caries," *Caries Res.* **18**, 540–547 (1984).

20. B. Angmar-Mansson and J. J. ten Bosch, "Optical methods for the detection and quantification of caries," *Adv. Dent. Res.* **1**, 14–20 (1987).

21. J. J. ten Bosch and J. C. Coops, "Tooth color and reflectance as related to light scattering and enamel hardness," *J. Dent. Res.* **74**, 374–380 (1995).

22. C. C. Ko, D. Tantbirojn, T. Wang, and W. H. Douglas, "Optical scattering power for characterization of mineral loss," *J. Dent. Res.* **79**, 1584–1589 (2000).

23. H. M. Theuns, R. P. Shellis, A. Groeneveld, J. W. E. v. Dijk, and D. F. G. Poole, "Relationships between birefringence and mineral content in artificial caries lesions in enamel," *Caries Res.* **27**, 9–14 (1993).

24. J. S. Wefel, B. H. Clarkson, and J. R. Heilman, "Natural root caries: a histologic and microradiographic evaluation," *J. Oral Pathol.* **14**, 615–623 (1985).

25. J. Vaarkamp, J. J. ten Bosch, and E. H. Verdonschot, "Light propagation through teeth containing simulated caries lesions," *Phys. Med. Biol.* **40**, 1375–1387 (1995).

26. J. D. B. Featherstone, M. M. O'Reilly, M. Shariati, and S. Brugler, in *Factors Relating to Demineralization and Remlneralization of the Teeth*, S. A. Leach, Eds., IRL Press, Oxford, UK (1986).

27. J. D. B. Featherstone, R. Glena, M. Shariati, and C. P. Shields, "Dependence of *in vitro* demineralization and remineralization of dental enamel on fluoride concentration," *J. Dent. Res.* **69**, 620–625 (1990).

28. B. C. Wilson and G. Adam, "A Monte Carlo model for the absorption and flux distribution of light in tissue," *Med. Phys.* **10**, 824–830 (1989).

29. L. Wang and S. L. Jacques, "Monte Carlo modeling of light transport in multi-layer tissues in standard C," Univ. Texas M.D. Anderson Cancer Center, Houston, TX (1992).

30. G. M. Hale and M. R. Querry, "Optical constants of water in the 200-nm to 200-μm wavelength region," *Appl. Opt.* **12**, 555–563 (1973).

31. G. D. Huynh, C. L. Darling, and D. Fried, "Changes in the optical properties of dental enamel at 1310-nm after demineralization," *Proc. SPIE* **5313**, 118–124 (2004).